Synthetic Metals 209 (2015) 369–376

Contents lists available at ScienceDirect

Synthetic Metals

journal homepage: www.elsevier.com/locate/synmet

Supercapacitor electrodes based on nano-polyaniline deposited on hollow carbon spheres derived from cross-linked co-polymers

Kuiwen Shen[a], Fen Ran[a,b,*], Xuanxuan Zhang[a], Chang Liu[a], Naijie Wang[a], Xiaoqin Niu[b], Ying Liu[a], Dingjun Zhang[a], Lingbin Kong[a], Long Kang[a], Shaowei Chen[b,*]

[a] State Key Laboratory of Advanced Processing and Recycling of Non-ferrous Metals, Lanzhou University of Technology, Lanzhou 730050, PR China
[b] Department of Chemistry and Biochemistry, University of California, 1156High Street, Santa Cruz, California 95064, USA

ARTICLE INFO

Article history:
Received 23 April 2015
Received in revised form 10 August 2015
Accepted 12 August 2015
Available online xxx

Keywords:
Co-polymer
Nano-polyaniline
Hollow carbon spheres
Supercapacitor

ABSTRACT

Nano-polyaniline (nano-PANI) was deposited on hollow carbon spheres (HCS) to prepare nano-PANI/HCS composites via in-situ chemical polymerization. The composites combined the high pseudocapacitance of nano-PANI and the excellent porous structure of HCS which were prepared by the carbonization of a cross-linked co-polymer, poly(styrene-*co*-divinylbenzene-*co*-methylacrylic acid). The structure and properties of the resulting composites were characterized by Fourier-transform infrared spectroscopy (FTIR) and nitrogen (N_2) adsorption measurements, and the electrochemical behaviors were examined in 1 M H_2SO_4 aqueous solution. Morphology was studied by scanning electron microscopy (SEM) and transition electron microscopy (TEM). SEM and FTIR characterizations reveal that nano-PANI was successfully deposited on the surface of HCS; and electrochemical tests indicated that the nano-PANI/HCS composites exhibited a high specific capacitance of 435.0 F g^{-1}, along with good long-term cyclic stability (≈60% retention after 2000 cycles).

1. Introduction

Supercapacitors, also known as electrochemical capacitors or ultracapacitors, have received considerable attention from both industrial and academic points of view in recent years due to their high power capability, long cycle life, safe operation and potential applications as primary power sources [1–3]. Because of its higher power density, supercapacitors have played an irreplaceable role in supplementing or even replacing batteries in many applications, such as mobile phones, electric vehicles, and so on [4–6]. Based on the energy storage mechanism, supercapacitors can be divided into two categories: electrochemical double-layer capacitors (EDLC) and pseudocapacitors, the latter of which include fast and reversible faradic reactions of electroactive materials [7–11]. In general, carbon that possesses high specific surface areas and good pore structures is the ideal EDLC electrode materials [12–19] that typically feature a high power density and excellent cycle- to-cycle stability. Nevertheless, the specific capacitance of carbon alone remains subpar as compared to those of other electrode materials.

Electrically conducting polymers, such as polyaniline (PANI) and polypyrrole, also have been extensively studied for pseudo-capacitor applications because of their low costs, fast redox rate, ease of synthesis and high theoretical capacitance. However, such polymers also have some fatal disadvantages: poor stability due to structural degradation through electrode redox processes, low conductivity and limited transport rates of anions [20–23]. Therefore, it has been proposed that composites based on conducting polymers and carbon may combine their respective advantages for enhanced capacitance performance [24–28].

Compared to other carbon materials, hollow carbon spheres (HCS) with unique pore structures show stupendous potential as EDLC electrode materials. HCS with a small size and high surface area can provide short diffusion paths and large electroactive regions, which are important for effective electrolyte transport to the electrode surface in supercapacitors [29–31] . In addition, good conductivity of HCS can also facilitate electron transport for faradic reactions of conducting polymers (e.g., PANI). Therefore, coating conducting polymers on the surface of HCS is a promising strategy to improve the overall capacitive properties by taking advantages of the intrinsic properties of HCS, such as good conductivity and high surface area [32–34]. Lei et al. synthesized PANI and porous carbon composites as electrode materials for supercapacitors by using chemical vapor deposition with ferrocene as the carbon precursor and colloidal silica spheres as the hard template, and

* Corresponding authors.
E-mail addresses: ranfen@163.com, ranfen@lut.cn (F. Ran), shaowei@ucsc.edu (S. Chen).

http://dx.doi.org/10.1016/j.synthmet.2015.08.012
0379-6779/

then by using chemical oxidative polymerization of aniline; a good specific capacitance performance of the composite material was obtained [35].

Herein, we report a facile and yet versatile approach to the synthesis of composite materials based on HCS and nano-PANI using a soft template method and in situ chemical polymerization. HCS, derived from a crosslinked co-polymer, not only play an important role in enhancing electrical conductivity, but also provide a large surface area for the deposition of nanoscale PANI particles. The electrochemical performance of the composite materials as supercapacitor electrodes was examined in 1 M H_2SO_4 aqueous solution. The correlation between the composite structures and electrochemical performance was also investigated and discussed in detail.

2. Experimental

2.1. Chemicals

Aniline (analytical reagent), styrene (St., analytical reagent) and methylacrylic acid (MAA, analytical reagent) was purchased from Aladdin Reagents Inc., and subject to distillation treatment prior to use. Ammonium persulfate (APS, analytical reagent) and trafluoroethylene (PTFE, 60 wt% dispersion in water) were also purchased from Aladdin Reagents Inc. and used as received.

2.2. Preparation of hollow carbon spheres (HCS)

2.2.1. Poly(styrene-co-methylacrylic acid) (P(St-co-MAA)) spheres

In a typical synthesis, MAA (0.431 g) was dispersed in distilled-water (100 mL) in a single-necked round-bottom flask, followed by the dropwise addition of St at room temperature under magnetic stirring in a nitrogen atmosphere. The mixture was then heated to 80 °C with the addition of APS (0.135 g) where polymerization took place for 24 h. After the reaction, the resulting P(St-*co*-MAA) spheres were centrifuged and washed with both ethanol and distilled-water, then dispersed in 150 mL of distilled-water.

2.2.2. Poly(styrene-co-divinylbenzene-co-methylacrylic acid) (P(St-co-DVB-co-MAA)) hollow spheres

The solution (100 mL) of P(St-*co*- MAA) spheres obtained above, water (55 mL) and APS (0.135 g, 0.50 mmol) were mixed in a single-necked round-bottom flask at room temperature under magnetic stirring in a nitrogen atmosphere for 30 min. A mixture of St (2.083 g), MAA (0.431 g) and DVB (0.078 g) was then added dropwise into the solution; and the polymerization continued at 80 °C for 24 h. After the reaction, the product was centrifuged and washed with both ethanol and distilled-water, then dispersed in 150 mL of DMF under stirring for 12 h. P(St-*co*-DVB-*co*-MAA) hollow spheres were obtained in a powder form by centrifugation, which were then washed with ethanol and distilled-water, and dried at 60 °C under vacuum for 24 h.

2.2.3. HCS

The P(St-*co*-DVB-*co*-MAA) synthesized above was first pre-oxidized at 320 °C in a muffle furnace for 5 h. After being cooled down to room temperature, the obtained product was then heated at 700 °C in a tube furnace under a nitrogen atmosphere for 2 h to remove the P(St-*r*-MAA) template spheres at a temperature ramp of 5 °C min^{-1}.

2.3. Preparation of nano-PANI/HCS

0.1 g nitric acid-treated HCS was immersed in 20 mL of an $HClO_4$ aqueous solution (1 M) under magnetic stirring and ultrasonic vibration for 30 min into which was added 10 mL of aniline (0.02 mol). The solution was mixed by ultrasonication for 30 min, and transferred into an ice water bath under stirring. When the solution temperature was 0 °C, APS (the molar ratio of aniline/APS was 1: 1) was added into the mixture dropwise and the mixture was stirred for a period of time (1, 3, 6 or 12 h). After polymerization, the composite was further washed by distilled water and ethanol until the filtrate solution was colorless and the pH was about 7. Finally, the composites were dried in vacuum oven at 60 °C for 24 h.

2.4. Characterization methods

The microstructures and morphology were examined by a scanning electron microscopy (SEM, Hitachi S-4800) and transition electron microscopy (TEM, JEOL JEM2010) measurements. FTIR spectra were acquired with a FTIR Nexus 670 instrument. Nitrogen (N_2) absorption and desorption isotherms were measured at 77 K by using a Micromeritics ASAP 2020 system. In addition, the specific surface area was determined by Brunauer–Emmett–Teller (BET) method and the pore size distribution was calculated by the Barrett–Joyner–Halenda (BJH) method using the adsorption branch of the isotherm. The electrical conductivities were performed using an in-line Four-Point Probes (RTS-4) and measured on pellets, which was prepared under a pressure of 20 MPa at room temperature (300 K).

2.5. Electrochemical analysis

To prepare electrodes for electrochemical tests, the composites prepared above, carbon black, conductive graphite, and PTFE were mixed at a weight ratio of 80: 7.5: 7.5: 5 to make a homogeneous black paste, which was then deposited onto the surface of a stainless steel grid and used as a current collector. The electrode was dried under vacuum at 60 °C for 6 h, and compressed at a pressure of 10 MPa to minimize the loss of electroactive materials during the electrochemical testing process.

Electrochemical measurements were conducted at room temperature in a traditional three-electrode configuration. The prepared electrode, a platinum gauze electrode, a saturated calomel electrode were used as the working, counter, and reference electrodes, respectively. The electrochemical tests were conducted in acidic solutions (1 mol L^{-1} H_2SO_4) to take advantage of the unique electrochemical behaviors of PANI in the composites in acidic solution. Electrochemical measurements were carried out with a CHI660C electrochemical workstation. Cyclic voltammograms were recorded between −0.2 and +0.8 V at different scan rates from 5 to 50 mV s^{-1}. For galvanostatic charge–discharge cycling, the current densities were varied from 0.5 to 5 A g^{-1} within the same potential range as in CV measurements and the specific capacitance was calculated from the discharging time and based on the formula $C = (I\Delta t)/(m\,V)$, where I is the discharging current and Δt is the time of discharge, m represents the mass of the active material and V is the potential window in acidic solution. Electrochemical impedance spectra were acquired with a frequency range of 1 to 10^5 Hz under a potential of −0.35 V. The cyclic stability measurement was carried out on a Land cell tester between −0.2 and +0.8 V for 2000 cycles.

3. Results and discussion

3.1. Synthesis mechanism of nano-PANI/HCS composite

The nano-PANI/HCS composites were synthesized by using in situ chemical polymerization of aniline on HCS. The preparation included the following five steps, as shown in Scheme 1. (i) Synthesis of poly (styrene-*co*-methylacrylic acid) (P(St-*co*-MAA))

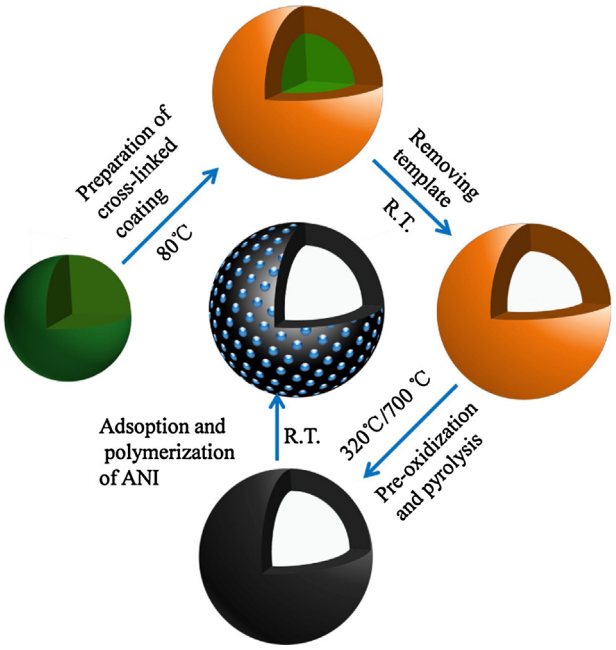

Scheme 1. Schematic illustration of the synthetic process of nano-PANI/HCS composites.

spheres as non-crosslinked templates; (ii) addition of a cross-linked copolymer layer of poly(styrene-*co*-divinylbenzene-*co*-methylacrylic acid) (P(St-*co*-DVB-*co*-MAA)) onto the surface of the template spheres; (iii) removal of the P(St-*co*-MAA) template spheres to obtain P(St-*co*-DVB-*co*-MAA) hollow spheres; (iv) pre-oxidation and subsequent pyrolysis of P(St-*co*-DVB-*co*-MAA) hollow spheres to obtain HCS; and (v) in situ deposition of PANI on HCS porous surfaces. The P(St-*co*-MAA) template spheres were prepared by emulsion polymerization of styrene and methylacrylic acid, and P(St-*co*-MAA)@P(St-*co*-DVB-*co*-MAA) core–shell spheres involving non-crosslinked core of P(St-*co*-MAA) and crosslinked shell P(St-*co*-DVB-*co*-MAA). In order to prepare porous hollow carbon spheres, the products were pre-oxidized at 320 °C for 5 h and subsequently pyrolyzed at 700 °C under a nitrogen atmosphere for 2 h. Finally, the nano-PANI/HCS composite were obtained by adsorption of aniline followed by in situ polymerization with APS. Note that to prepare high-performance electrode materials, it is important to control the monomer adsorption before polymerization and surface-modification steps, where surface modification helps HCS adsorb aniline easily and monomer adsorption helps aniline deposit on the porous surface of HCS uniformly.

The structures of the polymeric composites were first characterized by SEM and TEM measurement. As shown in the SEM image in Fig. 1a, hollow carbon spheres were obtained by carbonation of crosslinked co-polymers with the diameter about 240 nm and a relative smooth surface, which might be exploited for the deposition of nano-PANI. The SEM image in Fig. 1b clearly shows that PANI nanofibers were successfully grown on the HCS substrate to form a 3D cross-linked network structure. Fig. 1c and Fig. 1d are the corresponding TEM images of HCS and nano-PANI/HCS composite. The spheres in Fig. 1c displayed a hollow core and porous shell structure with the shell thickness about 30–50 nm. This thin porous shell afforded rapid diffusion of electrolyte ions into and out the shell layer, which is considered to be crucial for a high-rate supercapacitor [36]. After surface modification, the diameter and surface morphologies of HCS remained virtually unchanged (Fig. 1d). This indicates that indeed a layer of nano-PANI was formed on the HCS surface.

The incorporation of HCS and PANI in nano-PANI/HCS composite was then examined by FTIR measurements. FTIR spectra of HCS, pure PANI and nano-PANI/HCS composite are shown in Fig. 2. For HCS, the absorption bands at 1110, 1640 and

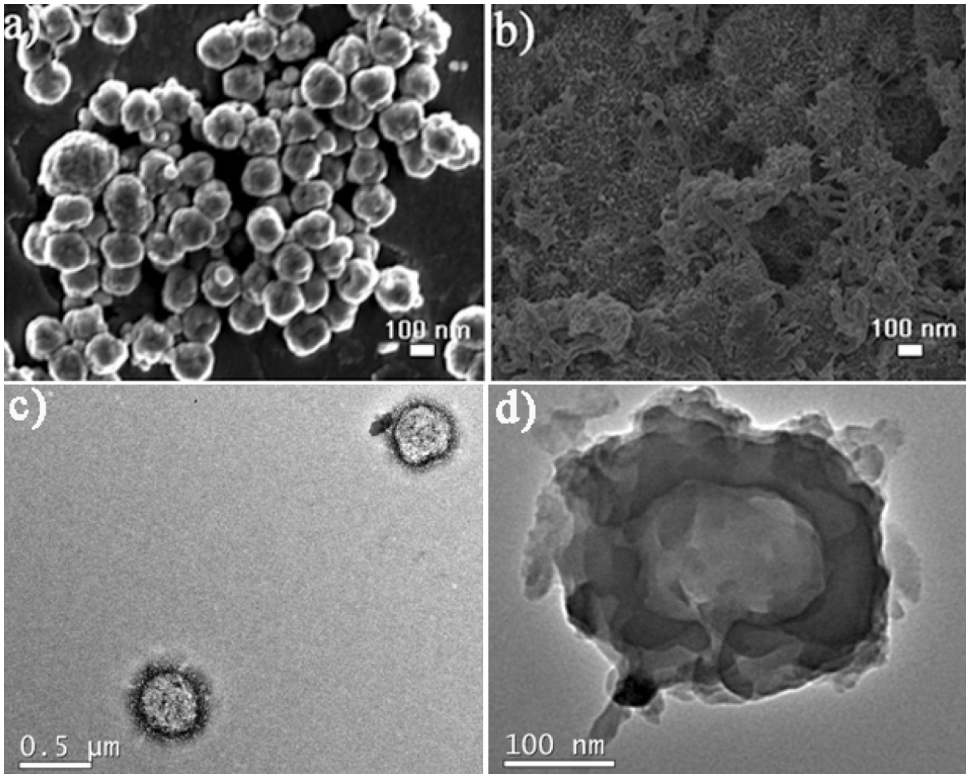

Fig. 1. Representative SEM images of a) HCS and b) nano-PANI/HCS composite prepared in the reaction time of 6 h; TEM images of c) HCS and d) nano-PANI/HCS composite.

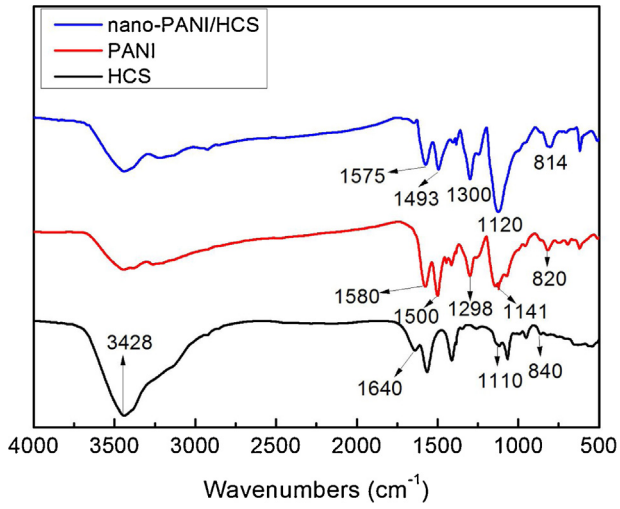

Fig. 2. The FTIR spectra of HCS (black curve), pure PANI (red curve) and nano-PANI/HCS composite (blue curve) synthesized in 6 h. (For interpretation of the references to color in this figure legend, the reader is referred to the web version of this article.)

3428 cm^{-1} can be assigned to the C—C—O, —OH and C=C stretching vibrations, respectively. The peak at 840 cm^{-1} can be ascribed to C—H vibration [28,37,38]. After polymerization of aniline, one can see several new vibrational features with the composite, such as 1575, 1493, 1300, 1120, and 801 cm^{-1}, as compared to HCS. The characteristic vibrations of the quinone (Q) and benzene rings at 1575 and 1493 cm^{-1}, which are representative of PANI, remained well- defined. For the nano-PANI/HCS composites, the peak at 1575 cm^{-1} is related to C=C stretching vibration modes of the quinonoid ring, while the peak at 1493 cm^{-1} is consistent with the phenyl C=C stretching [45]. The peaks at 1300, 1120 and 814 cm^{-1} are owed to the C—N stretching vibration of the secondary aromatic amine, N=Q=N stretching band and out of plane bending vibrations of C-H band in aromatic ring, respectively [28,39,45]. These results clearly indicate that nano-PANI was coated successfully on the HCS surface. As compared to the vibration characteristics (1580, 1500, 1298, 1141 cm^{-1}) of pure PANI, the peaks observed with the composite exhibited a clear blue shift, suggesting non-bonding interactions between PANI and HCS.

The textures of HCS and nano-PANI/HCS composite were investigated by N_2 adsorption. Fig. 3 shows the N_2 adsorption and desorption isotherms and pore size distribution on HCS and nano-PANI/HCS composite. In the isotherm curves of HCS, a linear increase in N_2 adsorption was observed in the low pressure range (P/P_0 = 0–0.1) due to the monolayer adsorption of N_2 molecules in the micropores [40], which gives rise to the high BET specific surface area value of 353 $m^2 g^{-1}$. In addition, a less obvious hysteresis loop occurred in desorption branch over the pressure range of P/P_0 = 0.35–0.9, indicating the existence of mesopores in the shell of HCS. The sharply increase of N_2 uptake in P/P_0 = 0.9–1.0 can be ascribe to the inter-particle voids and hollow cavity in the particle center [40]. These results indicated that coexistence of micropores, mesopores and macropores in HCS, which is consistent with the result of pore size distribution calculated by the BJH method (see in Fig. 3b). This interconnected porous feature is important for fast electrolyte wet and ion diffusion [41]. For nano-PANI/HCS composite, it is evident that coating PANI on the surface of HCS leads to dramatic decrease in the amount of N2 adsorbed (see in Fig. 3a). Meanwhile, the characteristic multimodal porosities, which can be observed for HCS, also disappeared and only the mesopores and macropores remained, suggesting an obvious pore blockage because of the coating of PANI on the surface of HCS. As a consequence, the BET specific surface area of nano-PANI/HCS composite was decreased to 8.3 $m^2 g^{-1}$. These observations were in good agreement with SEM analysis and TEM analysis (see in Fig. 1).

The effects of polymerization time of aniline on the surface morphologies of the composites were also investigated. Fig. 4 depicts the SEM images of nano-PANI/HCS composites prepared by polymerization of aniline for various periods of time. At 1 h of polymerization (Fig. 4a), the HCS surface became apparently roughened likely because of the formation and deposition of a thin layer of relatively short PANI nano-fibers on the HCS surface. With the reaction time increased to 3 h (Fig. 4b), PANI nano-fibers exhibited an increase of the size and density on the HCS surface. When the polymerization time was further increased to 6 h (Fig. 4c), the length of PANI nano-fibers became even longer and the diameter of PANI nano-fibers also larger. After 12 h of polymerization (Fig. 4d), we can see that the PANI nano-fibers became even cross-linked and did not form a uniform coating in the porous carbon surface. That is, this reaction time was too long to prepare well-defined nano-PANI/HCS composites.

3.2. Capacitive performances of HCS, pure PANI and nano-PANI/HCS composites

Cyclic voltammetry and galvanostatic charge–discharge tests were used to evaluate the supercapacitive performance of HCS, pure PANI and nano-PANI/HCS composite with a polymerization time of 6 h in three-electrode system. Fig. 5a shows CV curves of

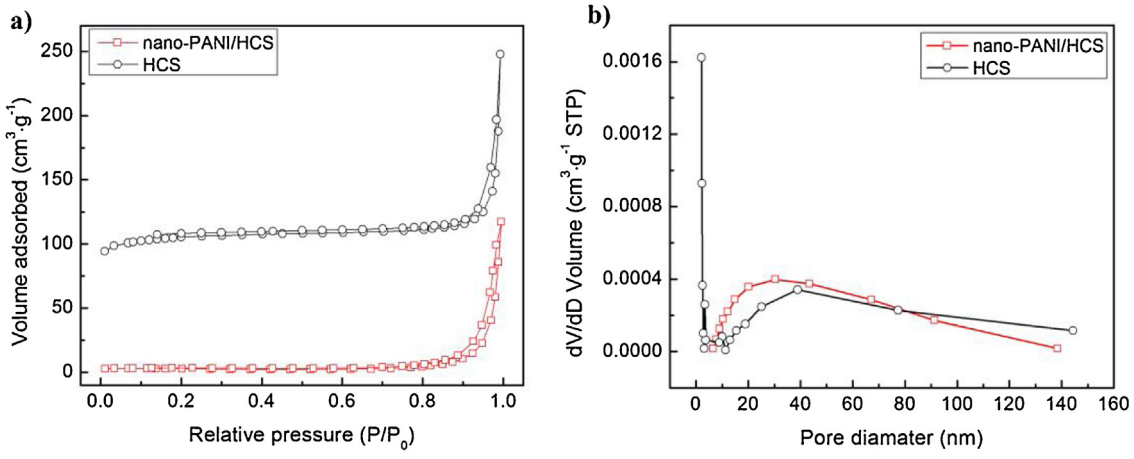

Fig. 3. a) N_2 adsorption and desorption isotherms and b) BJH pore size distribution curves of HCS and nano-PANI/HCS composite with a reaction time of 6 h.

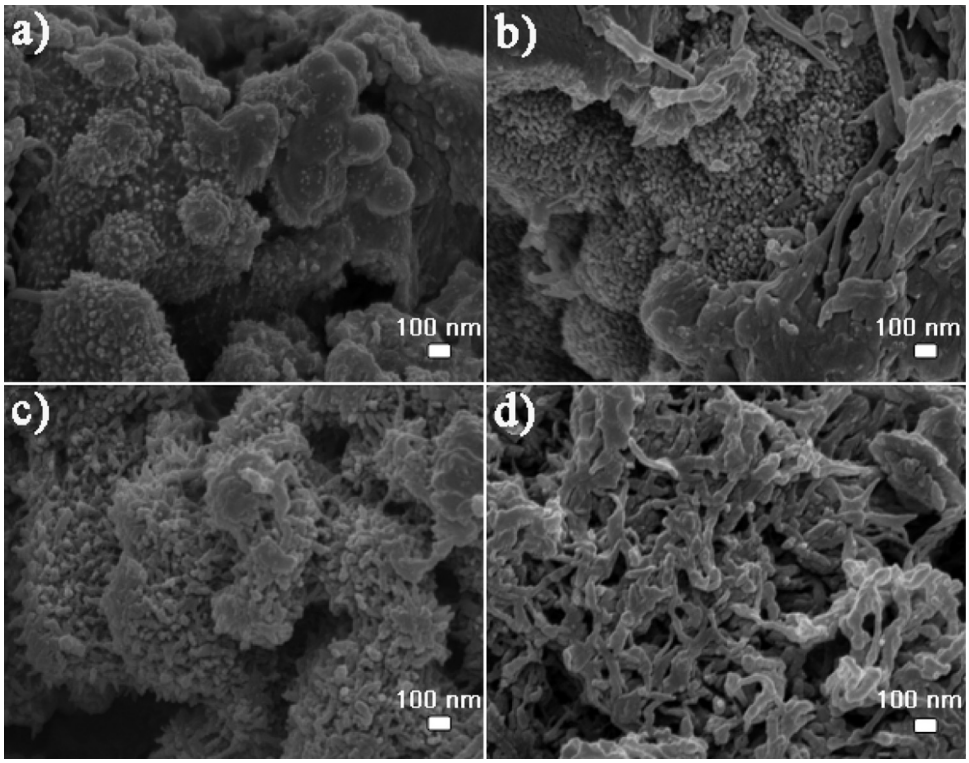

Fig. 4. SEM images of nano-PANI/HCS composites prepared at different reaction times: a) 1 h; b) 3 h; c) 6 h; and d) 12 h.

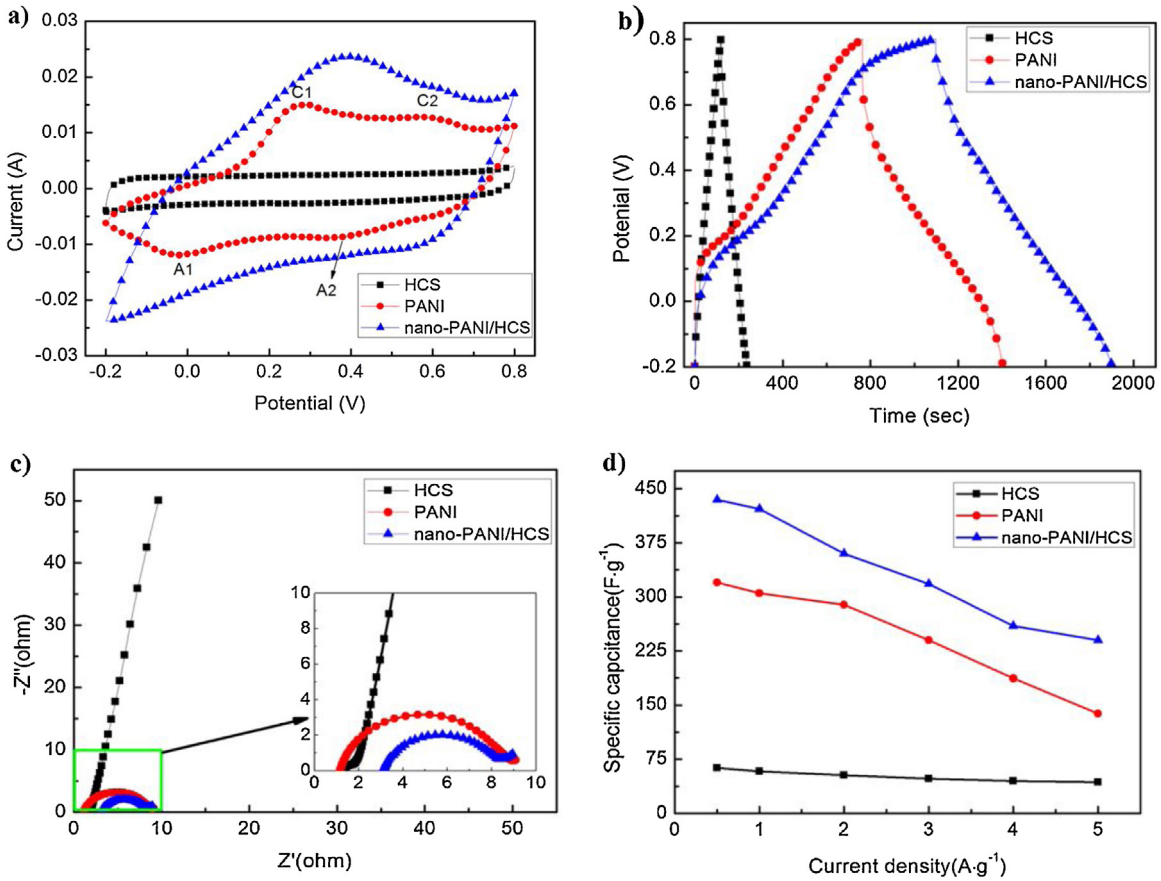

Fig. 5. Electrochemical performances of HCS, pure PANI, nano-PANI/HCS composite with a reaction time of 6 h in 1 M H_2SO_4. a) Cyclic voltammograms at a scan rate of 5 mV s^{-1}; b) galvanostatic charge–discharge curves at a current density of 0.5 A g^{-1}; c) Nyquist plots of the composite in a frequency range from 100 kHz to 1 Hz; and d) specific capacitance of active materials at different current densities.

HCS, PANI and nano-PANI/HCS composite between −0.8 and 0.2 V vs SCE measured at a sweep rate of 5 mV s^{-1}. The CV of pristine HCS exhibited almost perfect rectangular shape, implying that the energy is stored by the formation of electrochemical double-layer at electrode/electrolyte interface. For pure PANI, the redox peaks, which are the feature of pseudocapacitive behavior, obviously occurred in the CV curve. The peaks C_1/A_1 are corresponding to the redox transition of PANI between a semiconducting state (leucoemeraldine) and a conducting state (proton doped emeraldine), and another pair of peaks C_2/A_2 is due to the emeraldine-pernigraniline transformation [35] . Different from the CV curves of HCS and pure PANI, the nano-PANI/HCS composite CV curve contained humps as well as a rectangular shape, indicating that the capacitive response results from the combination of electrical double-layer formation and redox reactions. In addition, it is evident that the composite has a better charge storage capability because of wider area under CV curve. This agrees well with the long charge–discharge duration under the current density of 0.5 $A \cdot g^{-1}$ as shown in Fig. 5b. The gravimetric specific capacitance of HCS, pure PANI and composite were 63, 320, 435 $F \cdot g^{-1}$, respectively. The reversible redox reaction only happened on the surface of PANI [42] and the composite possesses unique structure properties with high surface area and hierarchically porous structure, so depositing PANI on the surface of HCS can really improve the utilization efficiency of PANI. The maximum specific capacitance of 435 $F g^{-1}$ can be obtained for nano-PANI/HCS composite. Moreover, the centered internal resistance (IR) drop of composite was observed at the beginning of discharge curve, confirming the decrease internal resistance owing to PANI chains covalent grafting to HCS. This conclusion can be further confirmed by electrochemical impedance spectroscopy. Typical Nyquist plots of HCS, pure PANI and nano-PANI/HCS composite at a frequency of 1–10^5 Hz are shown in Fig. 5c. The HCS displayed a single semicircle in the high-frequency region, whereas the almost vertical line in the low-frequency region implies the ideally capacitive behavior [43]. For pure PANI, the semicircle was quite large, suggesting this active material is certainly resistive. This phenomenon is partially caused by low conductivity of pure PANI, which shows an electrical conductivity of 0.48 S cm^{-1}. After coating PANI on the surface of HCS (the electrical conductivity of HCS is as high as 5 S cm^{-1}), the composite possesses an improved conductivity with a value of 1 S cm^{-1}, which can be explained for the small semicircle of composite in Fig. 5c and a smaller IR drop in Fig. 5b compared to pure PANI. Shown in Fig. 5d is the rate capability of HCS, pure PANI and nano-PANI/HCS composite over the current range of 0.5–5 A g^{-1}. All these three materials exhibited decreased capacitance retention at high current density, implying the increased diffusion resistance of electrolyte ions in the electrode materials [35]. The initial capacitance of HCS remained as high as 43 F g^{-1} even at a current density of 5 A g^{-1}, corresponding to 68.2% capacity retention. In contrast, the nano-PANI/HCS composite displays a decreasing capacitance retention of 55%. The capacitance loss was more pronounced with 43% retention of initial capacitance for pure PANI. The poor rate performance of pure PANI was probably caused by the pore blockage, which brings about less access of electrolyte ion to the surface of PANI, and the poor conductivity, which leads to high charge transfer resistance that acts as a limiting factor in faradic reactions [43].

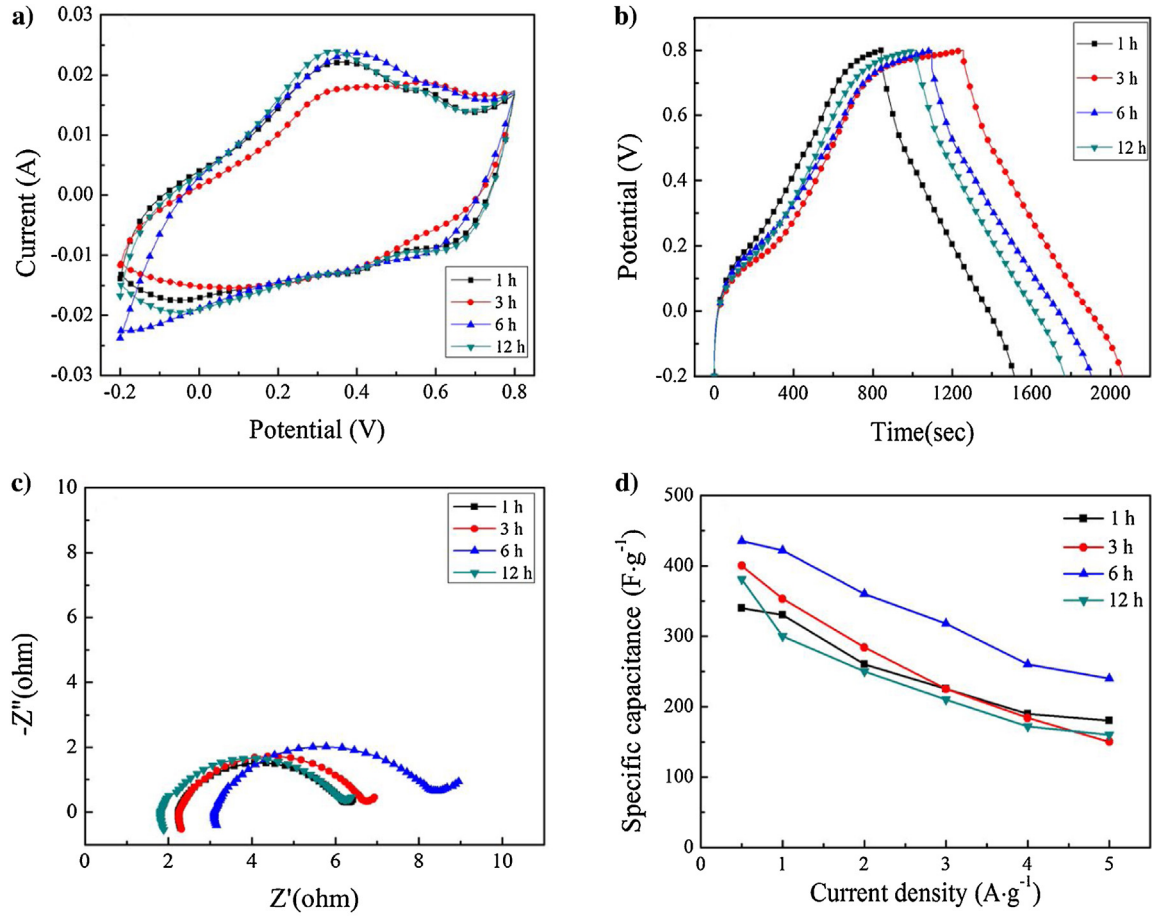

Fig. 6. Electrochemical performance of composites synthesized with different reaction time in 1 M H_2SO_4 solution. a) CV curves at the sweep rate 5 mV s^{-1}; b) galvanostatic charge–discharge curves at current density of 0.5 A g^{-1}; c) Nyquist plots; and d) specific capacitance at different current densities (0.5–5 A g^{-1}).

The capacitance performances of the composites prepared at different reaction times are shown in Fig. 6. As presented in Fig. 6a, all the CV curves under the same scan rate deviated from the rectangular shape and exhibit one pair of redox reaction peaks, indicating the contributions of pseudocapacitance and confirming the PANI coatings on the HCS surface. At longer reaction time, the redox peak became increasingly sharper and the voltammetric peak areas become larger. Also the galvanostatic charge–discharge curves of the composites at the same current density deviated somewhat from the linear symmetrical shapes (see Fig. 6b), similar to the CV curves. From these data, the highest specific capacitance value was estimated to be 435 F g^{-1} for the sample prepared after 6 h of polymerization. The decrease of the specific capacitance of the composites prepared at greater than 6 h, such as 12 h, due to the thick and nonuniform PANI layer formed that resulted in the low utilization efficiency of PANI. The charge transfer resistance and electrode-electrolyte resistance of composites prepared with different time were studied using EIS. A frequency respond analysis at open circuit potential over the frequency range from 10^5 to 1 Hz yielded the Nyquist plots shown in Fig. 6c. The semicircle region in high frequency range in Nyquist plot was related to the faradic resistance, which was modeled by a parallel combination of an interfacial charge transfer resistance [44]. The radiuses of semicircles at high frequency region of all composites were smaller than that of pure PANI (see Fig. 5c), indicating the charge transfer resistances were lower than that of pure PANI. Although this variation was small between different composites, the semicircle was gradually enlarged with the polymerization time of aniline, indicating that the material was more resistive. This change can be attributed to the much low conductivity of PANI in the composites. With the extension of polymerization time of aniline, the content of PANI in composites gradually increased and this given rise to a decreased conductivity of the composites. The decreased conductivity implied the slow charge transfer between active material and current density [35,43]. Fig. 6d shows the variation of the specific capacitance of the composites with current density ranging from 0.5 to 5 A g^{-1}. Even at the current density of 5 A/g, the specific capacitance of the composite of 6 h was 240 F g^{-1}, higher than 180 F g^{-1} of 1 h, 160 F g^{-1} of 3 h, and 160 F g^{-1} of 12 h. Again, one can see that the composite prepared in the reaction time of 6 h stood out with the best performance among the series.

For supercapacitors application, cycling stability is another important parameter. Therefore, durability tests over 2000 cycles were conducted at the current density of 4 A g^{-1} by galvanostatic charge–discharge measurements. From Fig. 7, it can be seen that nearly 60% of the initial capacitance is retained for the composite prepared in the reaction time of 6 h after 2000 cycles. As compared to pure PANI, it is apparent that the hybrids exhibits much enhanced cycle stability. After 500, 1000, 1500, 2000 cycles, the retention rates of the composite were 70, 61, 60, and 60%, respectively. The strong decrease of the specific capacitance at the beginning of cycle test can be attributed to the dopant replacement between the dopant of $HClO_4$ and the electrolyte of H_2SO_4. Furthermore, the composite became comparatively stable after 1500 cycles, which can be seen from the hardly changed value of the specific capacitance. The improved supercapacitive performance of composite may be contributed to the structural advantages. The unique HCS with a high surface area would improve the electrical conductivity and diffusion kinetics. In addition, the non-bonding interaction between PANI and HCS also plays an important role in cycle stability test.

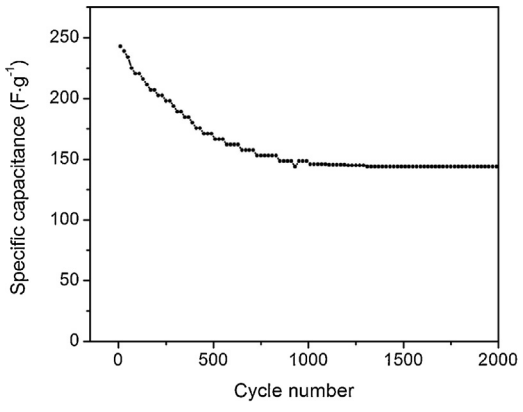

Fig. 7. Charge–discharge cycling at the current density of 4 A g^{-1} in 1 M H_2SO_4 solution.

4. Conclusion

In summary, hollow carbon spheres (HCS) consisting of porous shells were prepared by pyrolysis of core–shell crosslinked and non-crosslinked block copolymers. Due to the unique structure advantages, the HCS served as an excellent matrix for the growth of PANI. The nano-PANI/HCS composite was synthesized via in-situ chemical oxidative polymerization of aniline. Four composites with different PANI mass loadings were synthesized by adjusting the reaction time. The effect of polymerization time of aniline on morphologies and supercapacitor performances were studied in detail. The supercapacitive performance of nano-PANI/HCS composite is strongly relied on the mass of PANI on the HCS. When the polymerization time of aniline was 6 h, the maximum specific capacitance of 435 F g^{-1} was achieved. In addition, the composite electrode material also has a good cyclic stability (≈60% remain of initial capacitance after 2000 cycles). All these attractive features make this nano-PANI/HCS composites promising for supercapacitor applications.

Acknowledgements

This work was supported by the National Natural Science Foundation of China (51203071, 51363014, 51463012 and 51362018), China Postdoctoral Science Foundation (2014M552509, 2015T81064), the Opening Project of State Key Laboratory of Polymer Materials Engineering (Sichuan University) (sklpme2014-4-25), the Program for Hongliu Distinguished Young Scholars in Lanzhou University of Technology (J201402), and the University Scientific Research Project of Gansu Province (2014B-025).

References

[1] B. Andrew, Ultracapacitors: why, how, and where is the technology, J. Power Sources 91 (2000) 37–50.
[2] L.F. Lai, H.P. Yang, L. Wang, B.H. Teh, J.Q. Zhong, H. Chou, L.W. Chen, W. Chen, Z. S. Shen, R.S. Ruoff, J.Y. Lin, Preparation of supercapacitor electrodes through selection of graphene surface functionalities, ACS Nano 6 (2012) 5941–5951.
[3] L.L. Zhang, X.S. Zhao, Carbon-based materials as supercapacitor electrodes, Chem. Soc. Rev. 38 (2009) 2520–2531.
[4] G.Q. Zhang, X.W. Lou, General solution growth of mesoporous $NiCo_2O_4$ nanosheets on various conductive substrates as high-performance electrode for supercapacitors, Adv. Mater. 25 (2012) 976–979.
[5] X.C. Dong, X.W. Wang, J. Wang, H. Song, X.G. Li, L.H. Wang, M.B. Chan- Park, C. M. Li, P. Chen, Synthesis of a MnO_2-graphene foam hybrid with controlled MnO_2 particle shape and its use as a supercapacitor electrode, Carbon 50 (2012) 4865–4870.
[6] Jaidev, S. Ramaprabhu, Poly(p-phenylenediamine)/graphene nancomposites for supercapacitor applications, J. Mater. Chem. 22 (2012) 18775–18783.
[7] Y.T. Tan, F. Ran, L.R. Wang, Synthesis and electrochemical properties of hollow polyaniline microspheres by a sulfonated polystyrene template, J. Appl. Polym. Sci. 127 (2013) 1544–1549.
[8] M.C. Liu, L.B. Kong, C. Lu, X.M. Li, Y.C. Luo, L. Kang, X.H. Li, F.C. Walsh, A Sol-Gel process for the synthesis of $NiCo_2O_4$ having improved specific capacitance and

cycle stability for electrochemical capacitors, J. Electrochem. Soc. 159 (2012) A1262–A1266.
[9] L.Z. Fan, Y.S. Hu, J. Maier, P. Adelhelm, B. Smarsly, M. Antonietti, High electroactivity of polyaniline in supercapacitors by using a hierarchically porous carbon monolith as a support, Adv. Funct. Mater. 17 (2007) 3083–3087.
[10] F. Ran, H.L. Fan, L.L. Wang, A bird nest-like manganese dioxide and its application as electrode in supercapacitors, J. Energy Chem. 22 (2013) 928–934.
[11] P. Simon, Y. Gogotsi, Materials for electrochemical capacitors, Nature Mater. 7 (2008) 845–854.
[12] H.L. Fan, F. Ran, X.X. Zhang, H.M. Song, W.X. Jing, K.W. Shen, L.B. Kong, L. Kang, Easy fabrication and high electrochemical capacitive performance of hierarchical porous carbon by a method combining liquid–liquid phase separation and pyrolysis process, Electrochim. Acta 138 (2014) 367–375.
[13] R. Mysyk, Q. Gao, E. Raymundo-Pinero, F. Beguin, Microporous carbons finely-tuned by cyclic high-pressure low-temperature oxidation and their use in electrochemical capacitors, Carbon 50 (2012) 3367–3374.
[14] Y. Zhang, H. Feng, X.B. Wu, L.Z. Wang, A.Q. Zhang, T.C. Xia, H.C. Dong, X.F. Li, L.S. Zhang, Progress of electrochemical capacitor electrode materials: a review, Int. J. Hydrogen Energy 34 (2009) 4889–4899.
[15] C. Liu, F. Li, L.P. Ma, H.M. Cheng, Advanced materials for energy storage, Adv. Mater. 22 (2010) E28–E62.
[16] P.A. Goodman, H. Li, Y. Gao, Y.F. Lu, J.D. Stenger-Smith, J. Redepenning, Preparation and characterization of high surface area, high porosity carbon monoliths from pyrolyzed bovine bone and their performance as supercapacitor electrodes, Carbon 55 (2013) 291–298.
[17] Y.X. Xu, Z.Y. Lin, X.Q. Huang, Y. Wang, Y. Huang, X.F. Duan, Functionalized graphene hydrogel-based high-performance supercapacitors, Adv. Mater. 25 (2013) 5779–5784.
[18] X.R. Wen, D.S. Zhang, L.Y. Shi, T.T. Yan, H. Wang, J.P. Zhang, Three-dimensional hierarchical porous carbon with a bimodal pore arrangement for capacitor deionization, J. Mater. Chem. 22 (2012) 23835–23844.
[19] E. Frackowiak, F. Beguin, Carbon materials for the electrochemical storage of energy in capacitors, Carbon 39 (2001) 937–950.
[20] F. Ran, Y.T. Tan, J. Liu, L. Zhao, L.B. Kong, L. Kang, Preparation of hierarchical polyaniline nanotubes based on self-assembly and its electrochemical capacitance, Polym. Adv. Technol. 23 (2012) 1297–1301.
[21] H. Mi, X. Zhang, S. Yang, X. Ye, J. Luo, Polyaniline nanofibers as the electrode material for supercapacitors, Mater. Chem Phys. 112 (2008) 127–131.
[22] G.R. Li, Z.P. Feng, J.H. Zhong, Z.L. Wang, Y.X. Tong, Synthesis of hydrophilic nickel zinc ferrite thin films by chemical route for supercapacitor application, Macromolecules 43 (2010) 2178–2183.
[23] W. Chen, R.B. Rakhi, H.N. Alshareef, Facile synthesis of polyaniline nanotubes using reactive oxide templates for high energy density pseudocapacitors, J. Mater. Chem. A 1 (2013) 3315–3324.
[24] K.W. Shen, R. Fen, Y.T. Tan, X.Q. Niu, H.L. Fan, L.B. Kong, L. Kang, Toward interconnected hierarchical porous structure via chemical depositing organic nano-polyaniline on inorganic carbon scaffold for supercapacitor, Synth. Met. 199 (2015) 205–213.
[25] E. Frackowiak, V. Khomenko, K. Jurewicz, K. Lota, F. Beguin, Supercapacitors based on conducting polymers/nanotubes composites, J. Power Sources 153 (2006) 413–418.
[26] K. Lota, V. Khomenko, E. Frackowiak, Capacitance properties of poly(3, 4-ethylenedioxythiophene)/carbon nanotubes composites, J. Phys. Chem. Solids 65 (2004) 295–301.
[27] C. Arbizzani, M. Mastragostino, F. Soavi, New trends in electrochemical supercapacitors, J. Power Sources 100 (2001) 164–170.
[28] J. Hu, H.L. Wang, X. Huang, Improved electrochemical performance of hierarchical porous carbon/polyaniline composites, Electrochimica Acta 74 (2012) 98–104.
[29] H.M. Sun, L.Y. Cao, L.H. Lu, Bacteria promoted hierarchical carbon materials for high- performance supercapcitor, Energy Environ. Sci. 5 (2012) 6206–6213.
[30] T. Zhu, H.B. Wu, Y.B. Wang, R. Xu, X.W. Lou, Formation of 1D hierarchical structures composed of Ni_3S_4 nanosheets on CNTs backbone foe supercapacitors and photocatalytic H_2 production, Adv. Energy Mater. 2 (2012) 1497–1502.
[31] Y. Fan, P.F. Liu, Z.Y. Huang, T.W. Jiang, K.L. Yao, R. Han, Porous hollow carbon spheres for electrode material of supercapacitors and support material of dendritic Pt electrocatalyst, J. Power Sources 280 (2015) 30–38.
[32] M. Yang, G. Wang, Synthesis of hierarchical porous carbon particles by hollow polymer microsphere template, Colloids Surf. A 345 (1–3) (2009) 121–126.
[33] G.Y. Zheng, Y. Yang, J.J. Cha, S.S. Hong, Y. Cui, Hollow carbon nanofiber-encapsulated sulfur cathodes for high specific capacity rechargeable lithium batteries, Nano Lett. 11 (2011) 4462–4467.
[34] F.B. Su, X.S. Zhao, Y. Wang, L.K. Wang, J.Y. Lee, Hollow carbon spheres with a controllable shell structure, J. Mater. Chem. 45 (2006) 4413–4419.
[35] Z.B. Lei, C.Z. Wei, X.S. Zhao, Growth of polyaniline on hollow carbon spheres for enhancing electrocapacitance, J. Phys. Chem. C 114 (2010) 19867–19874.
[36] C. Liu, F. Li, L.P. Ma, H.M. Cheng, Advanced material for energy storage, Adv. Mater. 22 (2010) E28–E60.
[37] L. Gao, Y. Liao, X.H. Zhang, J.H. Chen, Preparation and enhanced electrocapacitive properties of polyaniline nanothorns on the surface of nitrogen-doped hollow carbon spheres, Chem. J. Chin. Univ. 34 (2013) 2845–2849.
[38] Y. Han, X.T. Dong, C. Zhang, S.X. Liu, Hierarchical porous carbon hollow-spheres as high performance electrical double-layer capacitor material, J. Power Sources 211 (2012) 92–96.
[39] M. Trchova, J. Stejskal, Polyaniline: the infrared spectroscopy of conducting polymer nanotubes (IUPAC Technical Report)*, Pure Appl. Chem. 83 (2011) 1803–1817.
[40] Z.C. Yang, C.H. Tang, H. Gong, X. Li, J. Wang, Hollow spheres of nanocarbon and their manganese dioxide hybrids derived from soft template for supercapacitor application, J. Power Sources 240 (2013) 713–720.
[41] H.Y. Liu, H.H. Song, X.H. Chen, S. Zhang, J.S. Zhou, Z.K. Ma, Effects of nitrogen- and oxygen-containing functional groups of activated carbon nanotubes on the electrochemical performance in supercapacitors, J. Power Sources 285 (2015) 303–309.
[42] J.R. Miller, P. Simon, Electrochemical capacitors for energy storage, Science 321 (2008) 651–652.
[43] V. Kumar, P.S. Lee, Redox active polyaniline-h-MoO_3 hollow nanorods for improved pseudocapacitive performance, J. Phys. Chem. C 119 (2015) 9041–9049.
[44] C. Portet, P.L. Taberna, P. Simon, C.L. Robert, Modification of Al current collector by sol-gel deposit for carbon-carbon supercapacitor applications, Electrochim. Acta 49 (2004) 905–912.
[45] H.S. Fan, H. Wang, N. Zhao, X.L. Zhang, J. Xu, Hierarchical nanocomposite of polyaniline nanorods grown on the surface of carbon nanotubes for high-performance supercapacitor electrode, J. Mater. Chem. 22 (2012) 2774–2780.